RSC Advances

PAPER

View Article Online
View Journal | View Issue

Cite this: *RSC Adv.*, 2024, **14**, 24105

Manganese tetraphenylporphyrin and carbon nanocoil interface-based electrochemical sensing of tyrosine†

Syeda Aqsa Batool Bukhari,[a] Abeera Aziz,[a] Habib Nasir,*[a] Sharif Ullah,[a] Tehmina Akhtar,[a] Sadia Iram,[ab] Effat Sitara,[ac] Shehla Mushtaq[ad] and Syed Abdul Moiz[e]

Tyrosine is one of the essential metabolites present in the human body for nutritional maintenance and normal physiological functioning. Its concentration in the body is crucial in predicting various hereditary, emotional, and physiological disorders. Therefore, quantitative monitoring of tyrosine in clinical samples is indispensable. We state the use of carbon nanocoils/manganese tetraphenylporphyrin convened glassy carbon electrode (CNC/MnTPP/GC) for the streamlined electrochemical sensing of tyrosine. Cutting-edge analytical techniques were employed to perform a comprehensive physicochemical analysis of the synthesized materials. To investigate the electrochemical properties, various techniques such as cyclic voltammetry (CV), differential pulse voltammetry (DPV), electrochemical impedance spectroscopy, and chronocoulometry were employed. CNC/MnTPP/GC displayed an optimal response at pH 5 and exhibited remarkable linearity within the concentration range of 0.05 to 100 μM for tyrosine. Using DPV, it demonstrated a low limit of detection (21 nM ± 1.17) and a sensitivity of 0.12 μA μM^{-1} cm^{-2}. CNC/MnTPP/GC displayed excellent performance in terms of repeatability, reproducibility, and stability for up to 30 days, making it suitable for real-time analysis, particularly in the analysis of tyrosine in blood serum. Notably, CNC/MnTPP/GC showcased a superior detection limit compared to previously reported methods.

Received 17th March 2024
Accepted 12th July 2024

DOI: 10.1039/d4ra02048k

rsc.li/rsc-advances

1. Introduction

Tyrosine plays a crucial role as a fundamental component in human biochemistry.[1] Along with its role in the production of proteins and melanin and the regulation of hormonal balance, tyrosine has a significant role in producing neurotransmitters in the body. Its concentration in the body assists in predicting various hereditary, emotional and physiological ailments such as hereditary tyrosinemia type I,[2] lung disorder[3] and cardiovascular diseases.[4] Hence, it is crucial to monitor the tyrosine concentration in the blood samples.

Several approaches are being utilized to estimate tyrosine[5] including spectrophotometric analysis,[6,7] chemiluminescence,[8] Raman spectroscopy,[9] GC-MS,[10,11] HPLC-UV,[12] ion-exchange chromatography[13] and fluorescence spectroscopy.[14] Although these methods provide an accurate and precise determination of tyrosine, they require sophisticated laboratory setups along with the tedious process to prepare the samples for analysis. This is the reason why electrochemical analysis has been selected to detect tyrosine more conveniently and does not require time-consuming preparation of samples similarly it is less expensive, has simple instrumentation, has good resolution, and proved to be effective in real-time analysis of the biomolecules.[15] A wide variety of combinations of nanomaterials are available to serve as electrode material to detect tyrosine and transduce signals efficiently in the form of readable output and these materials encompass non-/noble metal nanoparticles,[16] metallo-organic receptors[17] to carbon nanostructures[18] *etc.* Herein, we present the first-ever use of carbon nanocoils and MnTPP nanocomposite for the efficient detection of tyrosine.

Carbon nanocoils (CNC) are coiled structures that exist in a one-dimensional form, with diameters ranging from 10 to 100 nm and lengths varying from 10 to 100 mm. These CNCs have garnered significant interest in the realm of electrochemical analysis for applications such as sensors, supercapacitors, and fuel cells, primarily due to their distinctive chemical, mechanical, and optical properties.[19,20] The expansive specific surface area of carbon nanocoils enables the binding of receptor molecules through non-covalent interactions.

Metallo-porphyrins are planar macro heterocyclic molecules and are considered as bio-inspired organometallic compounds due to their rich electro-catalytic properties for redox reactions

[a]*Department of Chemistry, School of Natural Sciences, National University of Sciences and Technology, H-12, Islamabad, 44000, Pakistan. E-mail: habibnasir@sns.nust.edu.pk*

[b]*Department of Chemistry, Rawalpindi Women University, Rawalpindi, Pakistan*

[c]*Department of Chemistry, Karakoram International University, Gilgit, Pakistan*

[d]*Department of Chemistry, University of Management and Technology, Sialkot, Pakistan*

[e]*Department of Electrical Engineering, Umm Al-Qura University, Saudi Arabia*

† Electronic supplementary information (ESI) available. See DOI: https://doi.org/10.1039/d4ra02048k

of several classes of compounds like phenols *etc.*[21,22] Synthetic metalloporphyrins with different transition metals imitate the working mechanism of enzymes and provide good opportunities to be explored in the electrochemical sensing of organic and inorganic compounds.[23,24] Manganese tetraphenylporphyrin (MnTPP) and its derivatives exhibit excellent catalytic properties and have been used in electro-catalysis applications like water splitting and sensing of various organic compounds. The poor conductivity of tetraphenyl porphyrins limits their application to be used directly in electrochemical sensing devices, therefore, their composites with conducting substances like carbon nanomaterials are being used.

In the present research study, the nanocomposite of carbon nanocoils with manganese tetraphenylporphyrin was prepared and fully characterized. The charge transfer process at the surface of the as prepared electrode, CNC/MnTPP/GC, was studied using electrochemical impedance spectroscopy and chronocoulometry. Cyclic voltammetry and differential pulse voltammetry were employed to conduct tyrosine sensing studies under pH 5 conditions. The schematic representation is shown in Fig. 1.

2. Materials and methodology

2.1 Materials

Tyrosine, dopamine, uric acid, ascorbic acid, pyrrole (96%), potassium ferricyanide (99%), and manganese acetate (98%) were obtained from Sigma-Aldrich while disodium hydrogen phosphate (Na_2HPO_4), sodium dihydrogen phosphate (NaH_2PO_4), methanol (99%), ethanol (99.8%), chloroform (99%), propanoic acid (≥99.5%) and benzaldehyde were procured from Merck. Deionized water (DI) was used to prepare aqueous solutions. The electrode polishing kit consisting of 0.05 μm remained very useful for the polishing of GC.

2.2 Instrumentation

The attenuated total reflectance Fourier transform infrared spectrometer (Bruker, Alpha Platinum, Germany) was utilized for FTIR analysis, covering the range of 550–4000 cm^{-1}. The solid sample was analyzed using ATR-FTIR at room temperature. Raman analysis was conducted using the i-Raman high resolution TE Cooled Fiber Optic Raman System (Model: 1064 nm fiber optics, USA) with a wavelength of 532 nm, spanning the range of 150 to 4000 cm^{-1}. For Raman analysis powdered sample was used. UV-visible spectroscopic analysis of the materials was carried out using a PerkinElmer spectrometer (Model: Lambda-365) within the 250 to 700 nm region at room temperature and the solutions were prepared in DMF. To examine the morphology of the nanocomposites, a scanning electron microscope (SEM) (Jeol, JSM-6490A, Japan) was utilized, and the elemental composition of the materials was determined using energy-dispersive X-ray spectroscopy (EDS). SEM was conducted in at 20 kV and the powdered samples were coated with palladium. For the electrochemical experiments, including cyclic voltammetry (CV), differential pulse voltammetry (DPV), chronocoulometry, and electrochemical impedance spectroscopy (EIS), a Gamry 3000/3000AE workstation was employed. Throughout the electrochemistry experiments, a three-electrode system was utilized, consisting of a silver/silver chloride reference electrode filled with 0.3 M KCl, a platinum wire as the counter electrode, and a glassy carbon electrode as the working electrode.

2.3 Methodology

2.3.1 Synthesis of manganese tetraphenylporphyrin. The tetraphenylporphyrin synthesis was carried out using the Adler Longo method, as described in our previous work,[22] with the

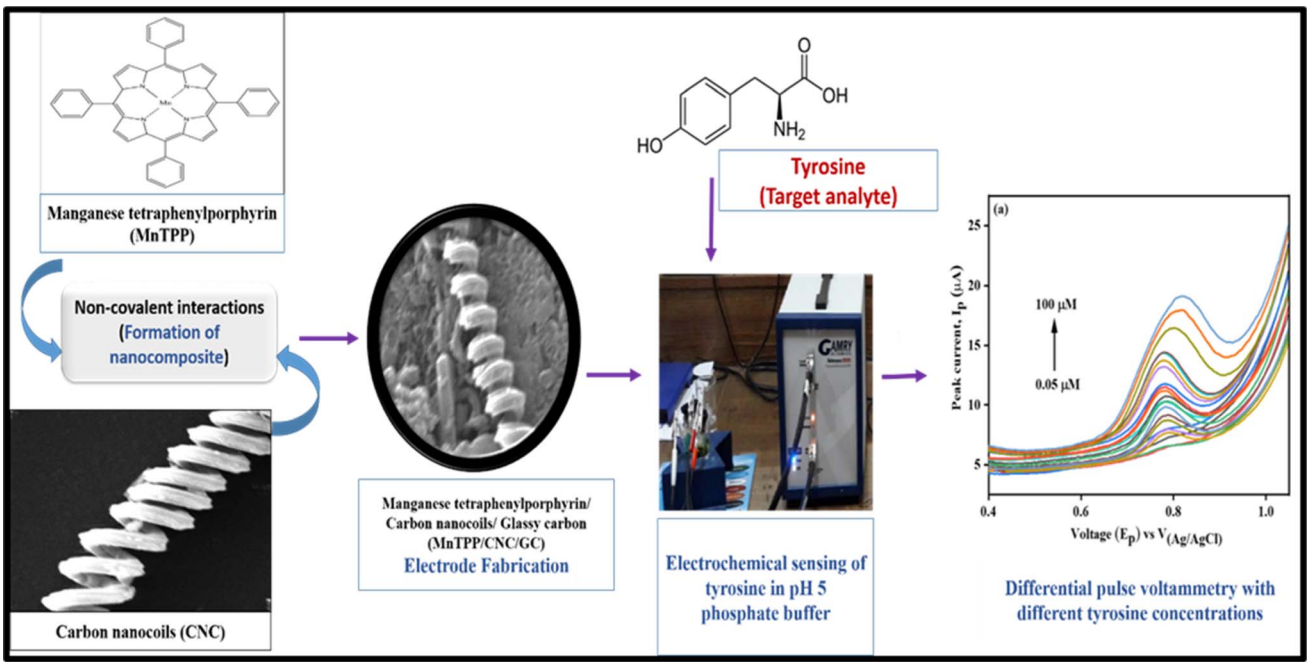

Fig. 1 Graphical representation of CNC/MnTPP/GC modified sensor for the electrochemical detection of tyrosine.

chemical structure presented in Fig. S1(a).† To synthesize manganese tetraphenylporphyrin, a reflux process was employed by adding TPP (100 mg in 50 mL chloroform) into a methanolic solution of manganese acetate (375 mg) and refluxing the mixture for 12 hours. TLC was used to monitor the reaction progress. Once the reaction was complete, the mixture was cooled, filtered, washed with chloroform, and dried under vacuum at 60 °C for 24 hours, resulting in a product yield of 78%. The chemical structure of the product is illustrated in Fig. S1(b).† [25]

2.3.2 Preparation of nanocomposite (CNC/MnTPP). To prepare the CNC/MnTPP nanocomposite, a dispersion was prepared by stirring CNC (5 mg) and MnTPP (15 mg) in DMF for 24 hours, followed by sonication for 3 hours. The synthesized CNC/MnTPP nanocomposite was then washed with ethanol *via* centrifugation and dried under vacuum at 60 °C for 24 hours. The modified glassy carbon electrode for electrochemical sensing was prepared by applying the CNC/MnTPP nanocomposite.

2.3.3 Glassy carbon electrode (GC) fabrication. Alumina polisher (0.05 μm) was employed for the polishing of GC, followed by sequential washing with ethanol, water, and acetone. Subsequently, the electrode was dried by purging it with nitrogen gas. A dispersion of CNC/MnTPP (2 mg) in 0.5 mL of DMF was prepared, and 8 μL of the suspension was carefully drop-casted onto the GC electrode. The resulting CNC/MnTPP/GC electrode was air dried. The same method was employed to fabricate the CNC/GC and MnTPP/GCE electrodes.

3. Results and discussion

3.1 Physicochemical characterization of the materials

Fig. 2 displays the Fourier transform infrared spectra of the materials prepared. The FTIR analysis of TPP reveals the existence of N–H stretching and bending vibration bands at 3314 cm^{-1} and 967 cm^{-1}, correspondingly.[26] The successful metalation of TPP was confirmed by observing the absence of N–H stretching and bending vibration bands at 3314 cm^{-1} and 967 cm^{-1}, respectively, as well as the presence of the Mn–N band at 1008 cm^{-1} in the FTIR spectrum of MnTPP.[27] CNC/MnTPP showed corresponding peaks for both CNC and MnTPP at 1540 cm^{-1} for aromatic C=C, at 1410 cm^{-1} for C=N, at 1331 cm^{-1} for C–N, and at 1001 cm^{-1} for Mn–N stretching vibrations but due to the formation of pi–pi interaction between carbon nanocoils and MnTPP the bands are shifted and somehow masked.

Raman analysis was performed for CNC, MnTPP, and CNC/MnTPP as shown in Fig. 3. It is well known that Raman of carbon nanostructured materials exhibit the characteristic D and G bands present at around 1300–1400 cm^{-1} and 1500–1600 cm^{-1}, respectively.[28,29] Weak band at 998 cm^{-1} is also present in the spectrum of MnTPP for the C_{ph}–H stretching that is shifted in the spectrum of CNC/MnTPP. Raman spectrum of CNC shows the presence of the intense bands *i.e.* D band at

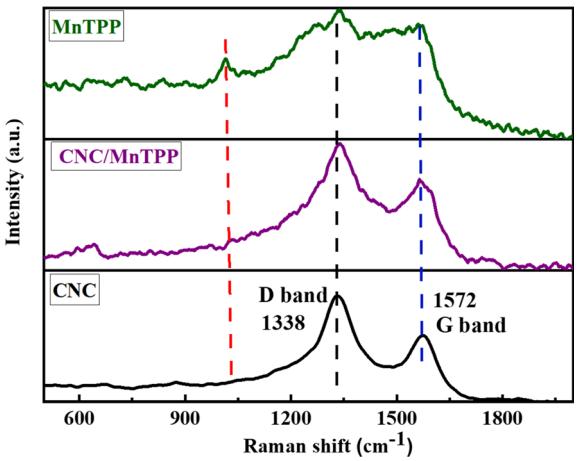

Fig. 3 Raman analysis of MnTPP, CNC/MnTPP, and CNC.

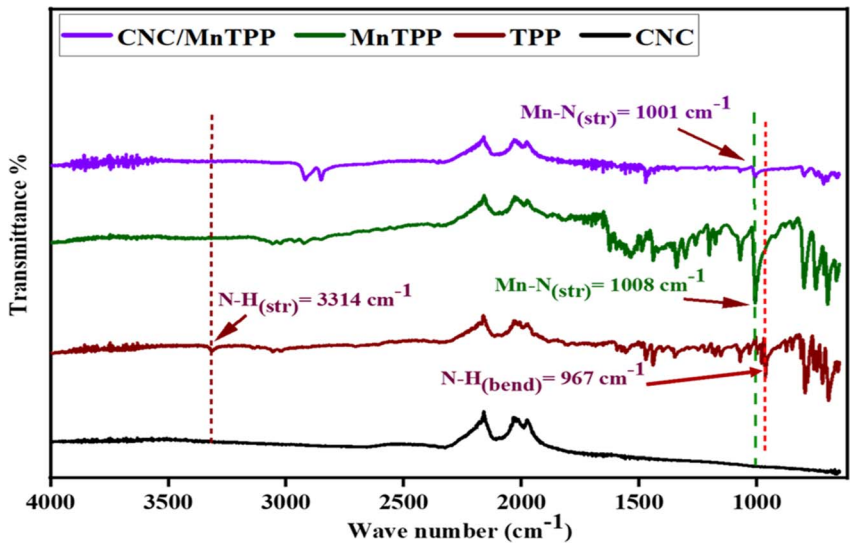

Fig. 2 FTIR of CNC/MnTPP, MnTPP, TPP, and CNC.

1338 cm^{-1} and G band at 1572 cm^{-1} representing somehow crystalline and amorphous structure of nanocoils with sp^3–sp^2 mixed character.[30] The shifting of bands in CNC/MnTPP as compared to the pristine MnTPP and CNC is an indication that the nanocomposite is formed due to the pi–pi conjugation between CNC and the MnTPP.

Ultraviolet-visible spectroscopy is helpful in the identification of chemically colored compounds. Tetraphenylporphyrin shows characteristic absorbance bands in the visible region with an intense Soret band present in the range of 300–500 nm and small Q-bands spanning 500 nm to 700 nm. Herein, the UV/vis. analysis of the samples was performed in DMF solvent. In Fig. 4 tetraphenylporphyrin shows a sharp Soret band at 418 nm arising from π–π* transitions involved in the molecule. The four Q-bands with weak absorption arise due to n–π* transitions and appear at 515, 548, 590, and 644 nm. After the complexation of TPP with manganese ion the absorption bands of MnTPP show a large bathochromic shift of the Soret band, as well as the number of Q-bands, decreased. MnTPP exhibits a Soret band located at 468 nm, accompanied by two additional bands at 373 nm and 397 nm.[31] Moreover, two Q-bands can be seen at 578 nm and 614 nm. The diminution in the Q-bands for MnTPP depicts the formation of a more symmetrical molecule. The presence of two extra bands at 373 nm and 397 nm is an indication that the Mn ion has been incorporated into the TPP macrocycle.[31] The nanocomposite, CNC/MnTPP, displays a bathochromic shift in both the Soret and Q-bands, attributed to the pi–pi interaction between the porphyrin ring and the carbon nanocoils.

Scanning electron microscopic (SEM) analysis of CNC/MnTPP has been shown in Fig. S2(a).† The coiled morphological structures show the presence of carbon nanocoils in the nanocomposite. The presence of Mn (weight% = 1.37) in the energy dispersive spectroscopy could be the indication that CNC/MnTPP nanocomposite is formed (Fig. S2(b)†).

3.2 Electrochemical characterization of modified electrodes

GC, MnTPP/GC, CNC/GC, and CNC/MnTPP/GC fabricated electrodes were subjected to analyze their electrochemical interfacial properties using an internal probe potassium ferricyanide and their electrocatalytic performance towards tyrosine in aqueous buffer (pH 5).

3.2.1 Electrochemical properties of electrodes. Modified electrodes were subjected to electrochemical impedance spectroscopy (EIS) to investigate the charge transfer at the interface between the heterogeneous electrode and electrolyte. The analysis was performed using 5 mM $K_3[Fe(CN)_6]$ in 0.1 M KCl with respect to the open circuit potential (OCP). The frequency range spanned from 100 kHz (initial frequency) to 0.1 Hz (final frequency), with a sweep rate of 50 mV s^{-1}, an AC voltage of 10 mV rms, and a fixed voltage of 0.287 V. The EIS data can be presented in the form of Nyquist and Bode plots, and in this discussion, we will focus on the Nyquist diagram, which allows for a comparison of the charge transfer processes among GC, MnTPP/GC, CNC/GC, and CNC/MnTPP/GC (Fig. 5).

Nyquist diagram consists of three main regions *i.e.* low frequency region, mid frequency region, and high frequency region. The high frequency region is associated with the presence diffusion-limited process (Warburg diffusion) and the low frequency region talks about the solution resistance (Ru) whereas the mid frequency region tells a picture about the resistance faced by the charge from the electrolyte to the electrode surface and known as charge transfer resistance (R_{ct}). It indirectly provides information about the conductivities of the electrode. R_{ct} values were predicted by the fitting of the EIS data with the Randles circuit. R_{ct} for GC, MnTPP/GC, CNC/GC, and CNC/MnTPP/GC are 5.9 kΩ, 12.3 kΩ, 2.8 kΩ, and 901.9 Ω, respectively; indicating the conductive nature of CNC and the catalytic performance of MnTPP in the nanocomposite CNC/MnTPP and showing least charge transfer resistance when compared to other prepared electrodes.

The electrochemical surface area of the electrodes was obtained from cyclic voltammetric analysis of GC, CNC/GC, MnTPP/GC, and CNC/MnTPP/GC in 5 mM potassium ferricyanide solution in 0.1 M KCl, as shown in Fig. S3.† Applying the Randles–Sevcik equation, we sorted the electrochemical surface

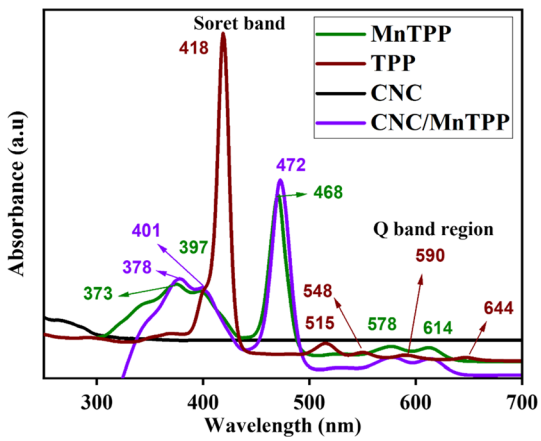

Fig. 4 UV-vis spectra of MnTPP, TPP, CNC, and CNC/MnTPP.

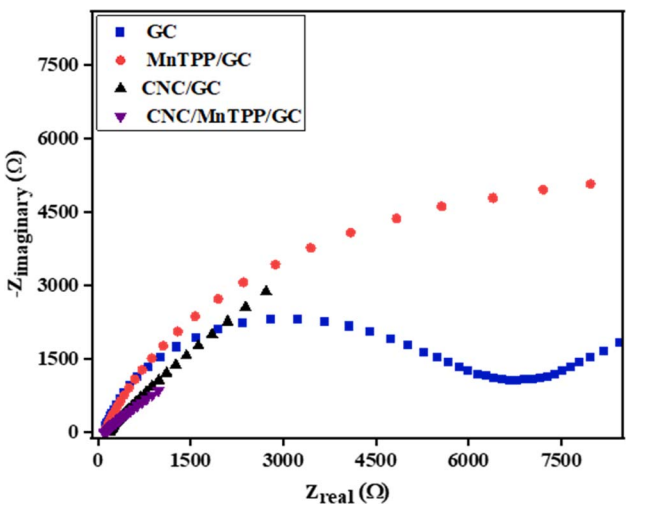

Fig. 5 Nyquist plot of GC, MnTPP/GC, CNC/GC, and CNC/MnTPP/GC in 5 mM potassium ferricyanide and 0.1 M KCl.

areas as; 0.007 cm^2, 0.019 cm^2, 0.025 cm^2 and 0.076 cm^2 for GC, MnTPP/GC, CNC/GC, and CNC/MnTPP/GC, respectively.

Chronocoulometric analysis (CC) also provides us with information on the more conductive nature of the CNC/MnTPP/GC electrode. CC was performed in the same conditions of potassium ferricyanide and potassium chloride electrolyte as EIS. CC curves demonstrate the change in the charge as a function of time for GC, MnTPP/GC, CNC/GC, and CNC/MnTPP/GC modified electrodes, as shown in Fig. 6. The lowest charge accumulation is observed for bare GC electrode (0.809 μC) and MnTPP (2.06 μC). When the GC is decorated with CNC and CNC/MnTPP, the amount of charge is increased from 9.80 μC to 21.91 μC as more active sites are available provided by both CNC and the nanocomposite. The amplified charge signal resulting from enhanced adsorption and accumulation of electroactive ferricyanide redox species on the electrode surface can be attributed to two factors: the high specific surface area provided by CNC and the increased electro catalytic ability of MnTPP.

3.2.2 Electroactivity of electrodes towards tyrosine. The electrochemical oxidation behavior of 100 μM tyrosine was probed in the phosphate buffer solution having the concentration of 0.1 M with pH 5 by voltammetric procedure (Fig. 7). No prominent oxidation peak was observed at both bare GC and MnTPP/GC in the presence of tyrosine due to the absence of any conducting support for MnTPP. The same experiment was also obtained at CNC/GC and CNC/MnTPP/GC in tyrosine and the oxidation process occurred. As there is no counter reduction peak in voltammograms so the electrochemical process of tyrosine is regarded as irreversible. At a potential of 0.79 V, tyrosine underwent oxidation, resulting in a peak intensity of 10.48 μA for CNC/MnTPP/GC. CNC/MnTPP/GC exhibited a higher current density compared to CNC, MnTPP/GC, and GC. This increase in current density was attributed to the combined effects of electron shuttling and the catalytic properties of carbon nanocoils and manganese centered tetraphenylporphyrin, which acted synergistically. Similarly, a significant

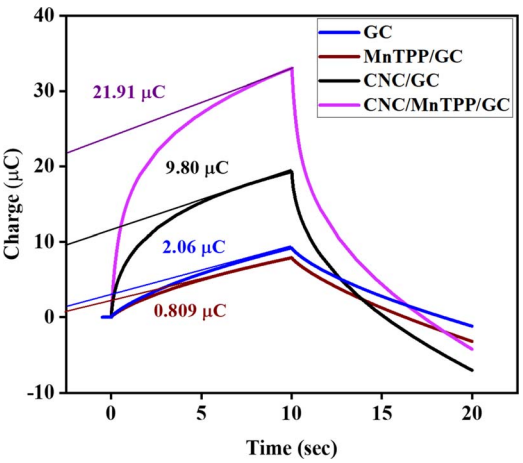

Fig. 6 Chronocoulometry of GC, MnTPP/GC, CNC/GC, and CNC/MnTPP/GC in 5 mM potassium ferricyanide and 0.1 M KCl (conditions; step 1 voltage = 0.3 V, step 1 time = 10 s, step 2 voltage = 0.1 V, and step 2 time = 10 s).

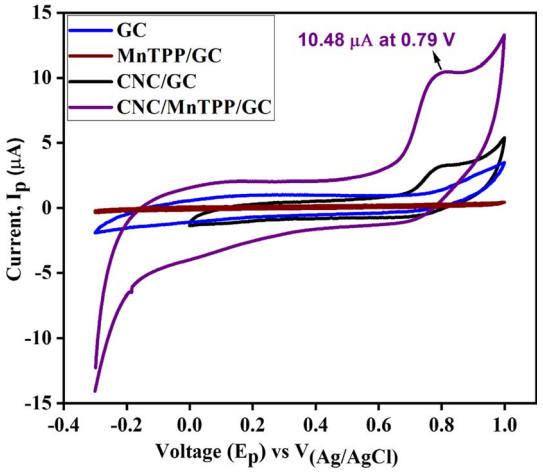

Fig. 7 Cyclic voltammograms of GC, MnTPP/GC, CNC/GC, and CNC/MnTPP/GC in 100 μM tyrosine in 0.1 M PBS (conditions; scan rate = 0.05 V s^{-1}; pH 5).

enhancement in the peak current of tyrosine is observed in CNC/MnTPP/GC and represents the excellent electrocatalytic nature of the fabricated electrode towards tyrosine. Therefore, all the remaining electrochemical studies were performed using CNC/MnTPP/GC sensor.

The sensitivity of CNC/MnTPP/GC sensors for detecting tyrosine can be influenced by the pH value, making it an important parameter in electrochemical detection. To examine this effect, cyclic voltammetry (CV) was conducted using a sodium hydrogen phosphate/sodium dihydrogen phosphate (PBS) buffer with pH values ranging from 3 to 8, shown in Fig. 8(a). The oxidation peak current of tyrosine exhibited an initial increase with rising pH, reaching its maximum at pH 5, followed by a decrease as the pH increased further. These findings indicate that the electrochemical behavior of tyrosine is pH-dependent, with the reaction rate at the electrode being influenced by the concentration of hydrogen ions. Additionally, the reduction peak potential shifted towards more negative values with increasing pH as shown in Fig. 8(b), suggesting the involvement of H^+ in the electrochemical reaction of tyrosine. This observation further confirms the reaction mechanism described in Scheme S1.† Consequently, a pH of 5 was chosen for subsequent experiments to investigate tyrosine detection.

Further, the kinetics of the electrode (CNC/MnTPP/GC) was analyzed by studying the effect of scan rate on the oxidation of tyrosine using CV. Increase in peak current is observed as the sweep rate increased from 0.01 V s^{-1} to 0.10 V s^{-1}, as illustrated in Fig. 9(a). The results of scan rate were assessed by making two linear relationships *i.e.* square root of scan rate ($\nu^{1/2}$) *vs.* peak current (I_{pa}) and logarithmic relationship between scan rate (ν) *vs.* peak current (I_p). The value of regression coefficient (R^2) obtained as a result of a plot of the square root of scan rate ($\nu^{1/2}$) *vs.* peak current (I_{pa}) was 0.98 (Fig. 9(b)), illustrating the charge transfer occurring at the surface of the electrode is due to the diffusion of tyrosine from the bulk to the surface of the electrode where the charge is transferred, and the analyte

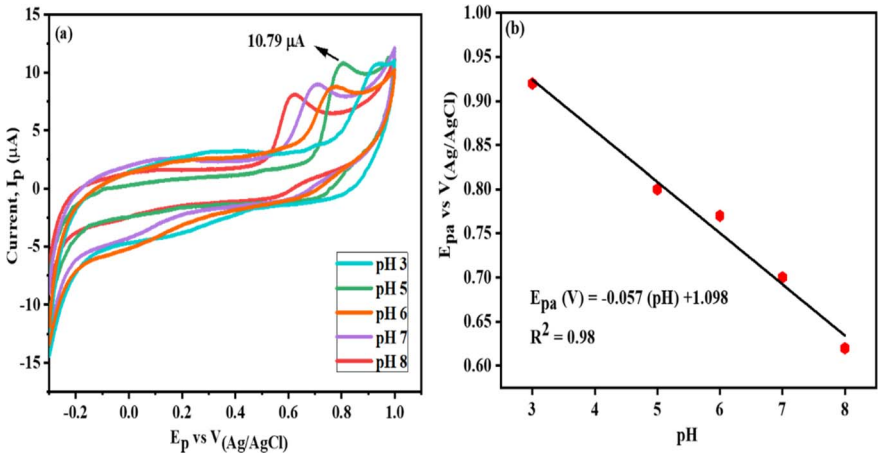

Fig. 8 (a) Effect of pH 3, 5, 6, 7 and 8 on CNC/MnTPP/GC in 100 μM tyrosine in 0.1 M PBS and (b) calibration plot for change in peak potential as well as peak current as a function of change in pH (pH 3, 5, 6, 7 and 8).

molecule is oxidized. The slope obtained from linear fitting of the log of scan rate *vs.* the log of the peak current Fig. 9(c) also provides useful information about the charge transfer process on the surface of the fabricated electrode. If slope is equal to 0.5 the electron transfer is occurring *via* diffusion process and if the slope is equal to 1 the charge transfer is due to the adsorbed material on the electrode thus showing an adsorption controlled mechanism. If this slope is between 0.5 and 1, then the process is both a mixed diffusion–adsorption controlled. From our experiments we can see the value of the slope is equal to 0.55, hence confirming the tyrosine detection at the electrode interface is diffusion controlled.

Similarly, it can be seen that as the scan rate increases, the peak potential also slightly shifts providing an indication of an

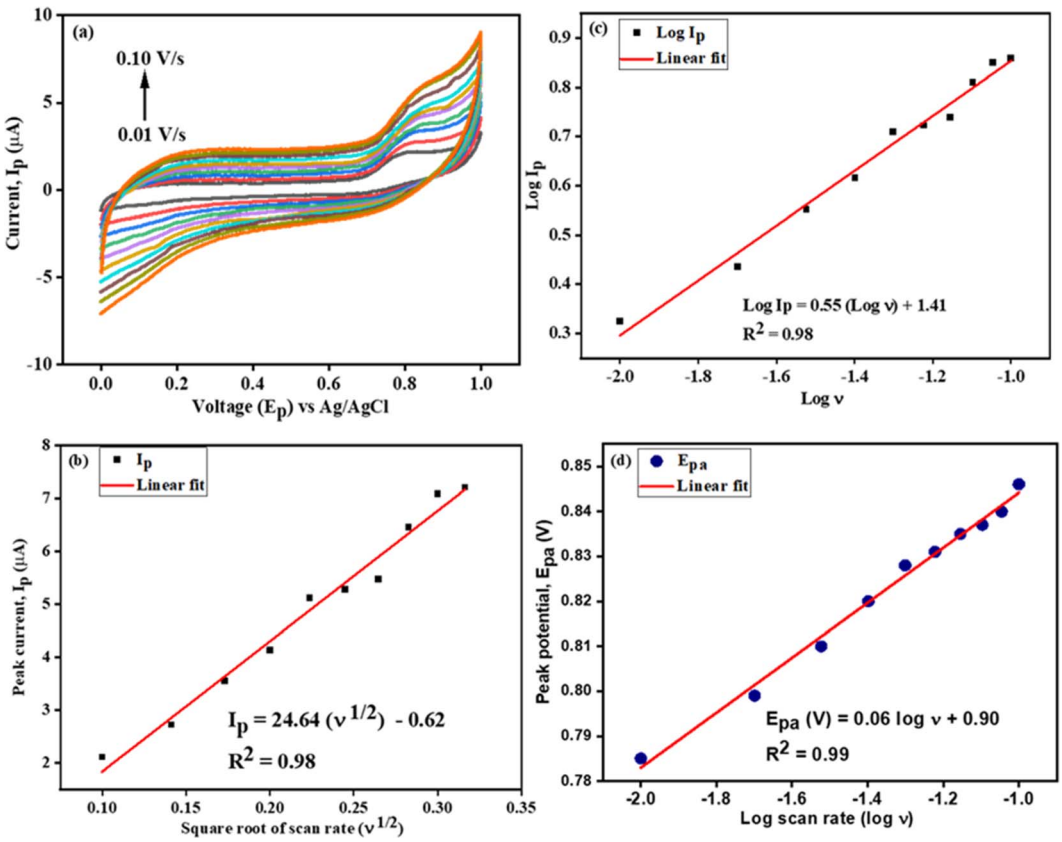

Fig. 9 (a) Effect of scan rate on CNC/MnTPP/GC in 100 μM tyrosine at pH 5.0 (b) calibration plot for change of current as a function of square root of scan rate, (c) log I_p *vs.* log ν and (d) E_{pa} *vs.* log ν.

irreversible electrocatalytic oxidation of tyrosine using CNC/MnTPP/GC electrode. Fig. 9(d) depicts the relationship between the (E_{pa}) and the log of scan rate ($\log \nu$) in the presence of tyrosine was developed. The regression equation is obtained as E_{pa} (V) = 0.06 $\log \nu$ + 0.90 (R^2 = 0.99) in the range from 0.01 to 0.1 V s^{-1}. The electrooxidation of tyrosine is an irreversible phenomenon so the Laviron equation is used to determine the relationship between $E_{pa,}$ and $\log \nu$ as shown in following equation:

$$E_{pa} = E^{\theta} + \frac{RT}{\alpha nF}\log\left(\frac{RT\ k^{\circ}}{\alpha nF}\right) + \frac{RT}{\alpha nF}\log \nu$$

Herein, α represents the charge transfer process, R is the gas constant, T is the temperature, F is the Faraday's constant, and n shows the number of electrons involved in the process. The value of $n\alpha$ is calculated from the slope of $\log \nu$ *vs.* E_p which is equal to 1.002. The transfer coefficient (α) was calculated using the equation *i.e.* $\alpha = 47.7/E_p - E_{p1/2}$ and obtained as 0.56. Further, the value calculated for n is 1.78 from $n\alpha$ which indicates that the tyrosine oxidation at the electrode surface is a two-electron irreversible process. The detail of the calculation is given in ESI above Scheme S1.†

Owing to the good electrochemical characteristics of the CNC/MnTPP/GC, its electrochemical behavior towards different concentrations of tyrosine was observed using both CV and differential pulse voltammetry (DPV). To account for CV curves for CNC/MnTPP/GC electrode in Fig. 10, the peak current is enhanced as the concentration of tyrosine is increased from 0.05 μM to 100 μM.

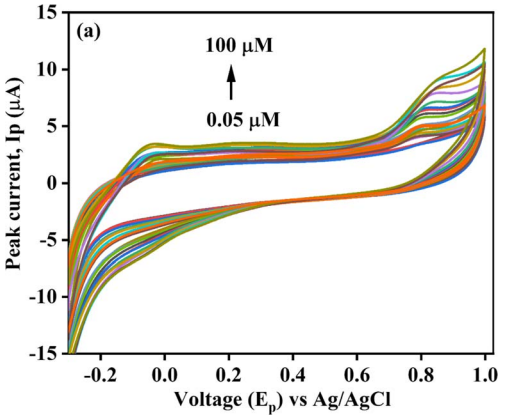

Fig. 10 CV of variable concentration of tyrosine (0.05 to 100.0 μM) on CNC/MnTPP/GC in 0.1 M PBS.

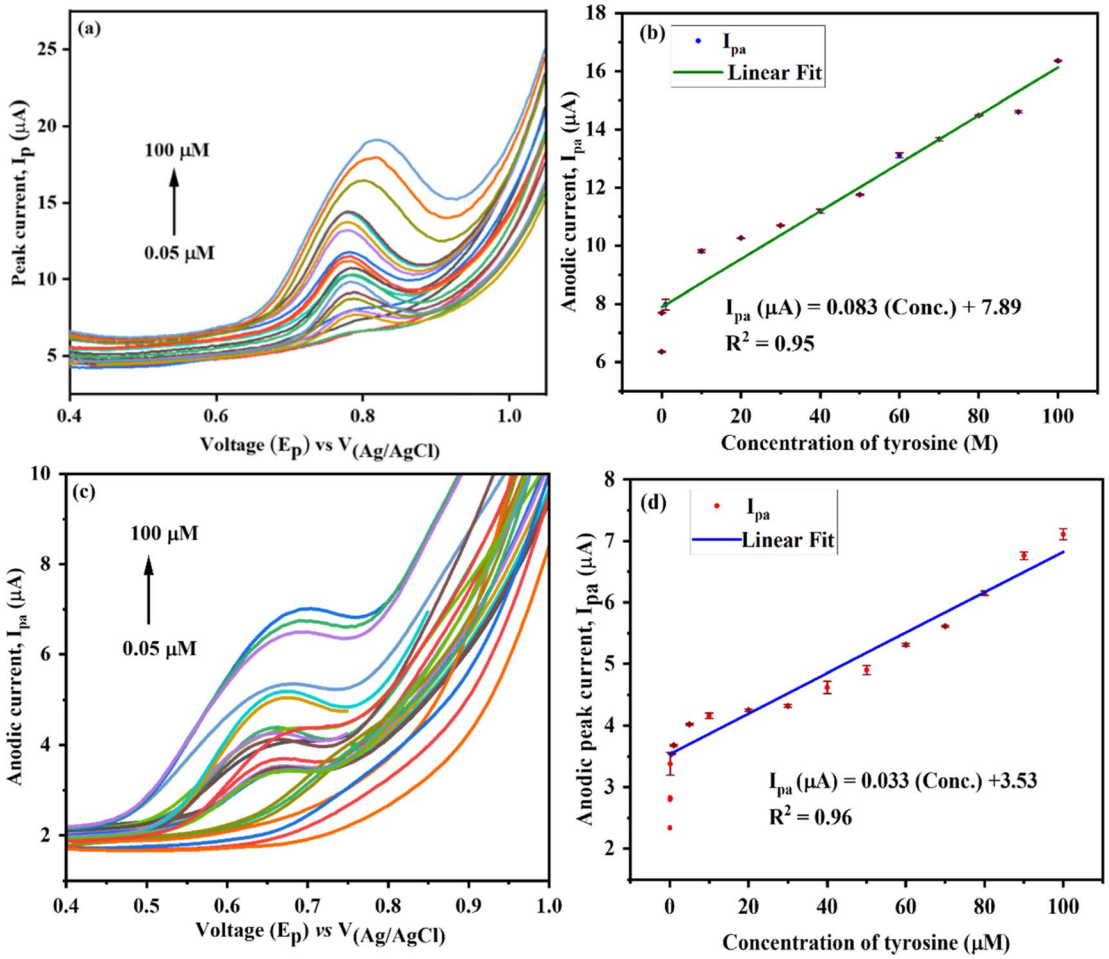

Fig. 11 DPV depicting the influence of varying concentrations of tyrosine (0.05 to 100 μM) on CNC/MnTPP/GC in 0.1 M PBS at (a) pH 5.0, (b) calibration plot at pH 5, (c) DPV at pH 7.4 and (d) calibration plot at pH 7.4.

Further, the DPV was conducted to notice the trend in CNC/MnTPP/GC sensor characteristics towards varied tyrosine concentrations *i.e.* 0.05–100 μM, as illustrated in Fig. 11(a) and (b). Again, to conclude for sensitivity measurement and the limit of detection, a linear trend was established between peak current and concentration of tyrosine. The sensitivity of the sensor was 0.12 μA μM^{-1} cm^{-2} and the limit of detection was 21 nM (±1.17). To generate a comparison between calibration plots taken at pH 5 and normal physiological pH 7.4 DPV was also performed for different concentrations of tyrosine at pH 7.4 (Fig. 11(c) and (d)). The linear concentration range studied was the same as for pH 5 but in pH 7.4 the anodic peaks started to appear from 0.1 μM concentration. LoD obtained was 45 nM (±1.58) with sensitivity as 0.43 μA μM^{-1} cm^{-2}.

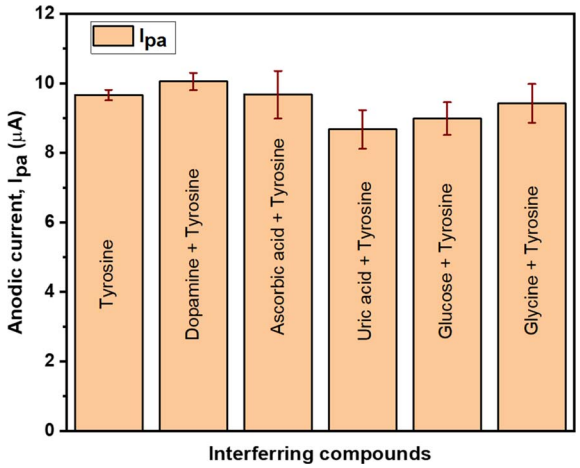

Fig. 12 Selectivity studies of CNC/MnTPP/GC sensor in 100 μM tyrosine solution (pH 5).

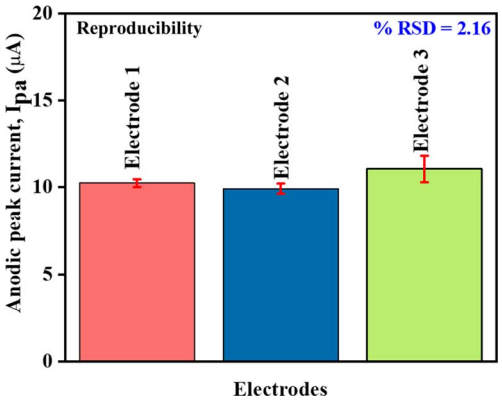

Fig. 13 Reproducibility studies of CNC/MnTPP/GC sensor in 100 μM tyrosine solution (pH 5).

3.2.3 Selectivity and reproducibility studies of CNC/MnTPP/GC. Bioanalytes such as uric acid, ascorbic acid, dopamine, glucose, and glycine which are also electroactive species for electrochemical measurement of tyrosine in their presence, were selected. It can be seen from Fig. 12, there is no or negligible interference on the current response of tyrosine by these analytes at a potential between 0.79 to 0.8 V. It represents the selective determination of tyrosine at the surface of the CNC/MnTPP/GC electrode. CNC/MnTPP/GC electrode has presented −4.03% tolerance for dopamine, −0.10% for ascorbic acid, +7.85% tolerance for uric acid, +4.96% tolerance for glucose, +0.41% for glycine as shown in Table S1.† Manganese ion present in the MnTPP most probably showed good interaction with tyrosine as compared to the other organic compounds in the specific potential range. Therefore, CNC/MnTPP/GC exhibited good selectivity values for tyrosine in the presence of other organic compounds.

Three different CNC/MnTPP/GC electrodes were prepared under identical conditions of ink deposition, drying temperature *etc.* The relative standard deviation incurred from the bar graphs in Fig. 13 is 2.16%, indicating excellent reproducibility of the prepared electrodes.

3.2.4 Repeatability and stability studies of CNC/MnTPP/GC electrode. In order to appraise the repeatability of newly fabricated CNC/MnTPP/GC sensor, we uninterruptedly scanned the sensor at 0.05 V s^{-1} for 7 times in 100 μM tyrosine solution (Fig. 14(a)). The quantification of current was done at a potential of 0.8 V. The relative standard deviation in the current sensitivity was 3.0%. The deviation was less than 5% thus signifies the good repeatability of the electrode.

We also reconnoitered the stability of the CNC/MnTPP/GC sensor. On the very first day, CV was performed in 100 μM

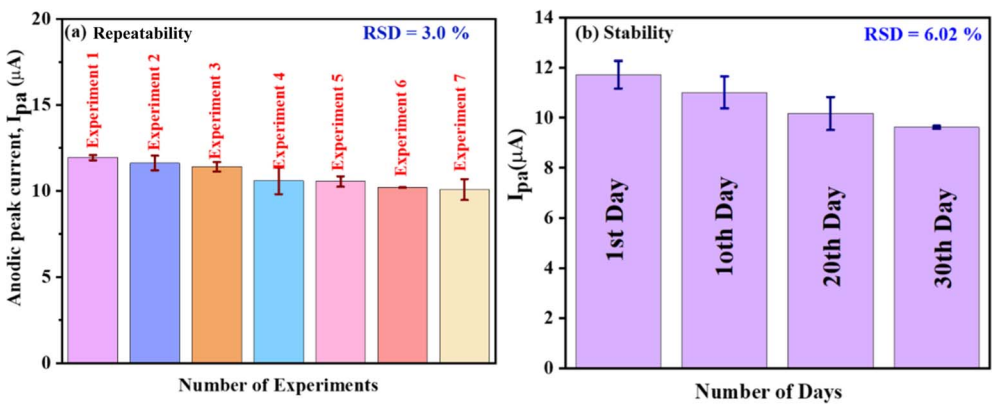

Fig. 14 (a) Repeatability studies and (b) stability experiment data of CNC/MnTPP/GC sensor in 100 μM tyrosine solution (pH 5).

Table 1 Determination of tyrosine in spiked blood serum samples using CNC/MnTPP/GC sensor (pH 5)

Serum sample	Added (μM)	Found (μM)	Recovery (%)	RSD (%)
Sample 1	40 μM	38.5 μM	96%	2.33 ($n = 3$)
Sample 2	50 μM	47.13 μM	94%	4.53 ($n = 3$)
Sample 3	60 μM	62.03 μM	103%	2.84 ($n = 3$)

tyrosine solution (pH 5). The tested modified electrode was stored for 10 days in the buffer solution in the refrigerator at 4 °C, tested, and again stored for further 10 more days, and so on till 30 days. The loss in current intensity was only 6%, indicating that CNC/MnTPP/GC possesses terrific stability (Fig. 14(b)).

3.2.5 Real sample analysis. Human blood serum was diluted with pH 5 phosphate buffer. Firstly, CNC/MnTPP/GC sensor was tested in the buffered serum and then the concentration of tyrosine was spiked into the buffered serum to scrutinize the performance of this newly developed sensor for practical applications. Table 1 depicts the summarized results.

3.2.6 Comparison of the performance of CNC/MnTPP/GC sensor with existing literature. The performance of the established sensor CNC/MnTPP/GC was compared to the already studied sensors in the literature as shown in Table S2.† CNC/MnTPP/GC exhibits good electrocatalytic activity towards tyrosine as compared to Sr. #1, Sr. #2, Sr #5 and Sr. #3. It is also to be noteworthy our sensor is easy to prepare and provides similar and nearby results as compared to the one described in Sr. #4.

4. Conclusions

A nanocomposite, CNC/MnTPP, was synthesized by incorporating manganese tetraphenylporphyrin onto the surface of carbon nanocoils. This nanocomposite was then drop-coated onto a GC electrode to enable the electrochemical detection of tyrosine. The electrochemical results demonstrated that CNC/MnTPP/GC exhibited excellent electrocatalytic activity for tyrosine. The combination of highly conductive CNC and MnTPP, which possesses exceptional electron transfer abilities, led to a notable synergistic catalytic effect in the electrocatalytic reaction of tyrosine. As a result, this novel composite holds great potential for applications in the electrochemical detection of tyrosine in biological fluids. CNC/MnTPP/GC exhibited significant linear response in a concentration range of 0.05 to 100 μM with a low limit of detection (21 nM ± 1.17) and sensitivity of 0.12 μA μM^{-1} cm^{-2}.

Author contributions

SABB: conceptualization, experimentation, methodology, investigation, writing – original draft and data curation; AZ: writing – original draft; HN: conceptualization, resources, supervision, validation, writing – review & editing, project administration and funding acquisition; SU: methodology and formal analysis; TA: formal analysis; SI: characterizations; ES: visualization and formal analysis; SM: formal analysis and experimentation; SAM: review and formal analysis.

Conflicts of interest

We declare no financial conflict of interests.

Acknowledgements

This research was supported by Pakistan Science Foundation under Project Number: PSF-NSFC/Eng-C-NUST (03). Authors are highly obliged to National University of Sciences and Technology, Islamabad, Pakistan for provision of lab facilities in order to accomplish our research endeavors. The authors would like to extend their gratitude to Prof. Lujun Pan from the Department of Physics at Dalian University of Technology in China for his kindness in providing carbon nanocoils for this research. We are also thankful to Pakistan Science Foundation Islamabad, Pakistan for the availability of funds for our research.

References

1 K. Moulaee and G. Neri, *Biosensors*, 2021, **11**, 502.
2 Y. Yang, Y. Song, X. Bo, J. Min, O. S. Pak, L. Zhu, M. Wang, J. Tu, A. Kogan and H. Zhang, *Nat. Biotechnol.*, 2020, **38**, 217–224.
3 J. T. Hartmann, M. Haap, H.-G. Kopp and H.-P. Lipp, *Curr. Drug Metab.*, 2009, **10**, 470–481.
4 A. B. Dollins, L. P. Krock, W. F. Storm, R. J. Wurtman and H. R. Lieberman, *Physiol. Behav.*, 1995, **57**, 223–230.
5 H.-Y. Zou, X.-Y. Lu, F.-Y. Kong, Z.-X. Wang, H.-Y. Li, H.-L. Fang and W. Wang, *RSC Adv.*, 2020, **10**, 28026–28031.
6 B. E. A. Basheir and A. A. Elbashir, *Chem. Express*, 2015, **8**, 95–101.
7 Y. Nozaki, *Arch. Biochem. Biophys.*, 1990, **277**, 324–333.
8 M. S. Alonso, L. L. Zamora and J. M. Calatayud, *Talanta*, 2003, **60**, 369–376.
9 Y. Lu, D. Lu, R. You, J. Liu, L. Huang, J. Su and S. Feng, *Nanomaterials*, 2018, **8**, 400.
10 A. L. Shroads, G. N. Henderson, J. Cheung, M. O. James and P. W. Stacpoole, *J. Chromatogr. B*, 2004, **808**, 153–161.
11 C. Deng, Y. Deng, B. Wang and X. Yang, *J. Chromatogr. B*, 2002, **780**, 407–413.
12 X.-m. Mo, Y. Li, A.-g. Tang and Y.-p. Ren, *Clin. Biochem.*, 2013, **46**, 1074–1078.
13 P. Allard, L. D. Cowell, T. H. Zytkovicz, M. S. Korson and M. G. Ampola, *Clin. Biochem.*, 2004, **37**, 857–862.
14 H. Yoshida, H. Nohta, Y. Harada, M. Yoshitake, K. Todoroki, K. Yamagata and M. Yamaguchi, *J. Chromatogr. B*, 2005, **821**, 88–93.
15 J. Zhang, J. Feng, Y. Tian, Y. Wu, X. Liu and Q. He, *Microchem. J.*, 2021, **171**, 106867.
16 Z. Wei, Y. Yang, X. Xiao, W. Zhang and J. Wang, *Sens. Actuators, B*, 2018, **255**, 895–906.
17 Q. Ma, S. Ai, H. Yin, Q. Chen and T. Tang, *Electrochicia Acta*, 2010, **55**, 6687–6694.
18 J. Wei, J. Qiu, L. Li, L. Ren, X. Zhang, J. Chaudhuri and S. Wang, *Nanotechnology*, 2012, **23**, 335707.

19 A. S. Khan, L. Pan, A. Farid, M. Javid, H. Huang and Y. Zhao, *Nanoscale*, 2021, **13**, 11943–11952.
20 S. Xu, Z. Fan, S. Yang, Y. Zhao and L. Pan, *Chem. Eng. J.*, 2021, **404**, 126064.
21 R. Peng, A. Offenhäusser, Y. Ermolenko and Y. Mourzina, *Sens. Actuators, B*, 2020, **321**, 128437.
22 S. A. B. Bukhari, H. Nasir, L. Pan, M. Tasawar, M. Sohail, M. Shahbaz, F. Gul and E. Sitara, *Sci. Rep.*, 2021, **11**, 1–13.
23 X. Guo, B. Guo, C. Li and Y. L. Wang, *J. Electroanal. Chem.*, 2016, **783**, 8–14.
24 Y. Yang, R. Sun, M. Li, B. Geng, J. Deng and M. Tang, *Int. J. Electrochem. Sci.*, 2016, **11**, 7370–7379.
25 S. Sakthinathan, H. F. Lee, S.-M. Chen and P. Tamizhdurai, *J. Colloid Interface Sci.*, 2016, **468**, 120–127.
26 Z. Qian-Kun and X.-X. Gao, *Electrochim. Acta*, 1995, **40**, 959–964.
27 K. Ezzayani, A. B. Khelifa, E. Saint-Aman, F. Loiseau and H. Nasri, *J. Mol. Struct.*, 2017, **1137**, 412–418.
28 E.-X. Ding, J. Wang, H.-Z. Geng, W.-Y. Wang, Y. Wang, Z.-C. Zhang, Z.-J. Luo, H.-J. Yang, C.-X. Zou and J. Kang, *Sci. Rep.*, 2015, **5**, 1–9.
29 C. Deng, P. Wang, C. Li, X. Wang and L. Pan, *Diamond Relat. Mater.*, 2019, **97**, 107426.
30 R. Cui, L. Pan, D. Li, H. Ma and W. Peng, *Carbon*, 2014, **76**, 455–458.
31 C. M. B. Neves, S. L. H. Rebelo, M. A. F. Faustino, M. G. P. M. S. Neves and M. M. Q. Simões, *Catalysts*, 2019, **9**, 967.